Carbon isotope discrimination of arctic and boreal biomes inferred from remote atmospheric measurements and a biosphere-atmosphere model

J. T. Randerson,[1] C. J. Still,[2] J. J. Ballé,[2] I. Y. Fung,[2] S. C. Doney,[3] P. P. Tans,[4] T. J. Conway,[4] J. W. C. White,[5] B. Vaughn,[5] N. Suits,[6] and A. S. Denning[6]

Received 10 May 2001; revised 2 December 2001; accepted 3 December 2001; published 2 July 2002.

[1] Estimating discrimination against ^{13}C during photosynthesis at landscape, regional, and biome scales is difficult because of large-scale variability in plant stress, vegetation composition, and photosynthetic pathway. Here we present estimates of ^{13}C discrimination for northern biomes based on a biosphere-atmosphere model and on National Oceanic and Atmospheric Administration Climate Monitoring and Diagnostics Laboratory and Institute of Arctic and Alpine Research remote flask measurements. With our inversion approach, we solved for three ecophysiological parameters of the northern biosphere (^{13}C discrimination, a net primary production light use efficiency, and a temperature sensitivity of heterotrophic respiration (a Q10 factor)) that provided a best fit between modeled and observed $\delta^{13}C$ and CO_2. In our analysis we attempted to explicitly correct for fossil fuel emissions, remote C4 ecosystem fluxes, ocean exchange, and isotopic disequilibria of terrestrial heterotrophic respiration caused by the Suess effect. We obtained a photosynthetic discrimination for arctic and boreal biomes between 19.0 and 19.6‰. Our inversion analysis suggests that Q10 and light use efficiency values that minimize the cost function covary. The optimal light use efficiency was 0.47 gC MJ^{-1} photosynthetically active radiation, and the optimal Q10 value was 1.52. Fossil fuel and ocean exchange contributed proportionally more to month-to-month changes in the atmospheric growth rate of $\delta^{13}C$ and CO_2 during winter months, suggesting that remote atmospheric observations during the summer may yield more precise estimates of the isotopic composition of the biosphere. *INDEX TERMS:* 0315 Atmospheric Composition and Structure: Biosphere/atmosphere interactions; 1851 Hydrology: Plant ecology; 9315 Information Related to Geographic Region: Arctic region; *KEYWORDS:* net primary production, light use efficiency, carbon isotope discrimination, temperature sensitivity of respiration, seasonal cycle of CO_2, Q10 respiration factor

1. Introduction

1.1. Background

[2] Precise measurements of discrimination against $^{13}CO_2$ during photosynthesis (denoted by Δ_A^{13}) are useful for assessing the impact of environmental variability on plant metabolism [*Evans et al.*, 1986; *Farquhar et al.*, 1989; *Lloyd and Farquhar*, 1994]. They are also required for analyzing the influence of terrestrial ecosystems on the atmospheric mass balance of $^{13}CO_2$ [*Battle et al.*, 2000; *Ciais et al.*, 1995; *Francey et al.*, 1995; *Keeling et al.*, 1995]. Yet, at ecosystem, landscape, and biome scales, estimates of Δ_A^{13} are relatively sparse and are subject to uncertainty arising from several sources.

[3] Two primary approaches for estimating ecosystem-scale Δ_A^{13} are (1) the extrapolation of isotopic measurements of plant and soil organic matter and (2) the analysis of the isotopic composition of CO_2 in air that is varying from biosphere-atmosphere gas exchange [*Keeling*, 1958, 1961]. In principal, the two approaches should yield equivalent estimates of Δ_A^{13} (from mass conservation), yet in practice, the two approaches frequently diverge. The Δ_A^{13} inferred from air sampling is sensitive to environmental conditions over a period of days to weeks [*Bowling et al.*, 2002; *Ekblad and Hogberg*, 2001], whereas plant and soil organic matter often reflect environmental con-

[1]Divisions of Geological and Planetary Sciences and Engineering and Applied Science, California Institute of Technology, Pasadena, California, USA.
[2]Center for Atmospheric Sciences, University of California, Berkeley, Berkeley, California, USA.
[3]Climate and Global Dynamics, National Center for Atmospheric Research, Boulder, Colorado, USA.
[4]Climate Monitoring and Diagnostics Laboratory, NOAA, Boulder, Colorado, USA.
[5]Institute of Arctic and Alpine Research, University of Colorado, Boulder, Colorado, USA.
[6]Department of Atmospheric Sciences, Colorado State University, Fort Collins, Colorado, USA.

0886-6236/02/2001GB001435$12.00

ditions over periods of months to years [*Buchmann et al.*, 1998].

[4] Isotopic measurements of plant and soil organic matter ($\delta^{13}C_b$) can be converted into photosynthetic discrimination (Δ_A^{13}) by removing an offset imposed by the atmosphere at the time of fixation ($\delta^{13}C_{atm}$) [*Farquhar et al.*, 1989]:

$$\Delta_A^{13} = \frac{\delta^{13}C_{atm} - \delta^{13}C_b}{1 + d^{13}C_b 1000}. \quad (1)$$

This approach also requires the critical assumption that discrimination in downstream processes such as construction, maintenance respiration, and decomposition is minimal or that discrimination and carbon fluxes associated with these processes can be explicitly accounted for [*Buchmann et al.*, 1998]. The challenge with implementing this approach at the biome scale comes from the wide variability of isotopic composition observed both between species and within individual plants [*Benner et al.*, 1987; *Korner et al.*, 1991; *Hayes*, 1993]. Sources of variation include species-to-species differences in photosynthetic pathway (i.e., C3 versus C4), discrimination in the biochemical formation of different plant compounds (i.e., lignin versus cellulose), leaf architecture (i.e., needles versus broad leaves), and environmental stress. In addition, use of equation (1) requires knowledge of the isotopic composition of the local atmosphere at the time of CO_2 fixation ($\delta^{13}C_{atm}$). This quantity is difficult to estimate because of diurnal and seasonal variability in the $\delta^{13}C$ of canopy and planetary boundary layer air [*Lloyd et al.*, 1996] and because of long-term changes in the isotopic composition of the global atmosphere (the ^{13}C Suess effect) [*Keeling et al.*, 1979]. Despite these limitations, plant functional types show consistent offsets in $\delta^{13}C_b$ that may serve as a basis for regional scale extrapolation of Δ_A^{13} [*Flanagan et al.*, 1996; *Brooks et al.*, 1997].

[5] Isotopic measurements of soil organic matter (SOM) have the advantage of integrating belowground net primary production (NPP) over a number of disturbance cycles [*Bird et al.*, 1996; *Tieszen et al.*, 1997]. However, spatial variability of soil ^{13}C within an ecosystem can be quite large [*Bird and Pousai*, 1997]. In addition, the relatively large mean residence time of bulk SOM leaves open the possibility that small levels of discrimination associated with decomposition, dissolved organic carbon leaching, or microbial C fixation could induce an offset over a number of years between the isotopic composition of SOM and soil CO_2 fluxes [*Ehleringer et al.*, 2000].

[6] The other widely used approach for estimating ecosystem-level Δ_A^{13} was developed by *Keeling* [1958, 1961]. With this approach, the isotopic composition of the source ($\delta^{13}C_b$) can be estimated from the intercept of a linear regression between measured atmospheric $\delta^{13}C$ (at time t and height z) and the reciprocal of the concentration CO_2 (t, z):

$$\delta^{13}C(t, z) = \delta^{13}C_b + \frac{M}{CO_2(t, z)}, \quad (2)$$

where M is also obtained from the regression and represents the product of the background CO_2 concentration and the difference between the isotopic composition of $\delta^{13}C_b$ and the isotopic composition of the background air. Once $\delta^{13}C_b$ is known, Δ_A^{13} can be estimated by removing the mean isotopic composition of the atmosphere at the time of fixation ($\delta^{13}C_{atm}$) using equation (1). However, as with the plant and soil isotope sampling approach, it is difficult to quantify $\delta^{13}C_{atm}$, because it requires knowledge of the distribution of ages of CO_2 emitted as ecosystem respiration (and the concurrent time history of $\delta^{13}C$ in the local atmosphere). The Keeling plot approach combines the discrimination of various elements within an ecosystem (and between various ecosystems within a region) in proportion to their contribution to the total biosphere-atmosphere CO_2 flux.

[7] Use of equation (2) requires the assumption of mixing between an atmospheric reservoir with a uniform composition and an isotopically homogeneous source or sink. At many scales of interest, however, this assumption does not always apply, even over the course of a single set of flask measurements. At the ecosystem scale, autotrophic and heterotrophic respirations may have different isotopic signatures. If these components contribute differentially during the course of a measurement, the regression intercept will be difficult to interpret. Other approaches, including relaxed eddy accumulation [*Bowling et al.*, 1999], the use of additional isotopic constraints ($\delta^{18}O$) [*Yakir and Wang*, 1996], and canopy-planetary boundary layer (canopy-PBL) models [*Lloyd et al.*, 1996], may be used to isolate multiple isotopic sources.

[8] At larger spatial scales, such as those sampled by aircraft [*Nakazawa et al.*, 1997; *Zahn et al.*, 2000; *Lloyd et al.*, 2001] or by remote flask networks [*Mook et al.*, 1983; *Trolier et al.*, 1996], variation in the isotopic composition of CO_2 will always have contributions from both photosynthesis and ecosystem respiration, along with contributions from ocean exchange [*Gruber and Keeling*, 2001; *Quay et al.*, 1992; *Tans et al.*, 1993] and fossil fuels [*Andres et al.*, 1996]. Where available, CO and $^{14}CO_2$ can be used to estimate the impact of fossil fuel contributions to the air measured at a particular flask station [*Bakwin et al.*, 1998], and radon (^{222}Rn) may be used to distinguish between air masses with oceanic and terrestrial origin [*Schmidt et al.*, 1996; *Zaucker et al.*, 1996].

1.2. This Study

[9] Here we estimate the isotopic composition of net seasonal CO_2 exchange ($\delta^{13}C_n$) at high northern latitudes by analyzing National Oceanic and Atmospheric Administration Climate Monitoring and Diagnostics Laboratory (NOAA/CMDL) and Institute of Arctic and Alpine Research (INSTAAR) flask measurements north of 50°N from 1993 to 1996. As defined here, $\delta^{13}C_n$ includes fossil fuel, ocean, and remote C4 ecosystem components in addition to seasonal exchange from terrestrial ecosystems. We estimate and remove minor contributions to $\delta^{13}C_n$ from ocean, fossil fuel, and remote C4 ecosystem fluxes, using an atmospheric model and prescribed surface fluxes. With a coupled biosphere-atmosphere model that includes time delays for heterotrophic respiration, we then solve for the optimal combination of three biosphere parameters, Δ_A^{13},

Table 1. NOAA/CDML and INSTAAR Flask Measurements Used in This Study

	Abbrev	Station	Country	Latitude	Longitude	Elevation, m	CO_2 Seasonal Amplitude ppm	$\delta^{13}C$ Seasonal Amplitude, ‰
1	ALT	Alert, Northwest Territories	Canada	82°27′N	62°31′W	210	14.08	0.75
2	ZEP	Ny-Alesund, Svalbard	Norway/Sweden	78°54′N	11°53′E	475	14.25	0.72
3	MBC	Mould Bay, Northwest Territories	Canada	76°15′N	119°21′W	15	14.57	0.79
4	BRW	Point Barrow, Alaska	United States	71°19′N	156°36′W	11	15.87	0.81
5	STM	Ocean Station "M"	Norway	66°00′N	2°00′E	6	14.80	0.71
6	ICE	Heimaey, Vestmannaeyjar	Iceland	63°15′N	20°09′W	100	13.86	0.71
7	BAL	Baltic Sea	Poland	55°30′N	16°40′E	7	15.98	0.79
8	CBA	Cold Bay, Alaska	United States	55°12′N	62°43′W	25	15.77	0.88
9	MHD	Mace Head, County Galway	Ireland	53°20′N	9°54′W	5	13.52	0.74
10	SHM	Shemya Island	United States	52°43′N	74°06′E	40	16.23	0.89

NPP light use efficiency (ε), and a Q10 factor (a temperature sensitivity parameter for respiration that is defined in section 2.5) that provide a best fit with the NOAA/CMDL and INSTAAR CO_2 and $\delta^{13}C$ data. We define Δ_A^{13} as a flux-weighted photosynthetic discrimination, integrated over the entire growing season, for northern biomes including boreal forest and arctic tundra. Our analysis builds upon previous work by *Knorr and Heimann* [1995], where optimal NPP and Q10 values were estimated by using biosphere and atmosphere models and seasonal CO_2 observations, and is comparable in approach with *Kaminski et al.* [2002].

[10] There are several advantages to initially focusing our analysis on high northern latitudes. First, while understanding the contribution of C4 photosynthesis to global NPP is an essential prerequisite to partitioning ocean and land carbon sinks using atmospheric $^{13}CO_2$ [*Fung et al.*, 1997; *Lloyd and Farquhar*, 1994; *Still et al.*, 2002], it is also important to characterize spatial and temporal variation in discrimination by C3 vegetation. While there are several C4 species present in boreal forest biomes, their abundance (and thus their contribution to NPP and net ecosystem production (NEP)) is small [*Schwarz and Redmann*, 1988; *Collatz et al.*, 1998], allowing us to isolate the isotopic composition of the C3 end-member. Second, as compared with midlatitude, tropical, and Southern Hemisphere regions, in the far north the terrestrial biosphere is the dominant contributor to seasonal variation in CO_2; fossil fuel and ocean contributions to seasonal variation are minor [*Heimann et al.*, 1998; *Randerson et al.*, 1997]. The large seasonal amplitudes of both CO_2 and $\delta^{13}C$ in the north facilitate removal of the long-term secular trend caused primarily by fossil fuels and allow for relatively low levels of uncertainty in retrieval of ecophysiological parameters.

2. Methods

2.1. Atmospheric Data Selection and Trend Removal

[11] We used monthly mean data (available at http://www.cmdl.noaa.gov/ccg/) from all available NOAA/CMDL and INSTAAR remote flask stations north of 50°N (Table 1) [*Trolier et al.*, 1996]. These northern stations are influenced mostly by arctic and boreal biomes on seasonal timescales [*Kaminski et al.*, 1996]. We only included data points in our analysis when monthly mean CO_2 and $\delta^{13}C$ were simultaneously available.

[12] A smoothing spline was used to remove the low-frequency secular trend at each station [*Enting*, 1987]. After the secular trend was removed, we truncated each time series at the beginning and end by 7 months to remove any edge effects induced from the spline. A single mean value for each station, obtained from the average of the low-frequency spline fit, was added back to each point in the time series for use with equation (2). We restricted our analysis of the detrended time series to the period between January 1993 and December 1996. We chose this 4-year period because most stations were sampled during this time, allowing a retrieval of biosphere parameters that was not strongly biased by variations in station density.

2.2. The Isotopic Composition of Net Seasonal CO_2 Exchange

[13] With the detrended monthly station data, we estimated the isotopic composition of net seasonal CO_2 exchange, $\delta^{13}C_n$, using equation (2) (Table 2). We accomplished this using a type II regression program that accounted for errors associated with both the CO_2 and $\delta^{13}C$ measurements and that provided standard error estimates for both the slope and intercept regression parameters [*Press et al.*, 1992]. This regression approach generally gives more negative $\delta^{13}C_n$ intercepts than type I regressions where the independent variable is assumed to have no error [*Sokal and Rohlf*, 1980].

[14] At each station, we estimated $\delta^{13}C_n$ (1) using all available data (January–December), and we also estimated separately for (2) summer (May–September) and (3) winter (October–April) periods (Table 2). In the regression procedure each monthly data point was assigned a standard error of 0.2 ppm for CO_2 and 0.05‰ for $\delta^{13}C$ to approximately capture the atmospheric variation in weekly flask measurements that contribute to the filtered monthly mean [*Trolier et al.*, 1996]. We estimated $\delta^{13}C_n$ for the combination of all stations by pooling all of the detrended station data together in the regression analysis.

2.3. Construction of a Multistation Time Series North of 50°N

[15] We made a combined time series for all of the stations north of 50°N from January 1993 to December 1996 by averaging all available station data at each monthly time interval described in section 2.1. Since not all of the stations were active during each time interval, the number of

Table 2. Isotopic Composition of Net Seasonal CO_2 Exchange ($\delta^{13}C_n$) From 1993 to 1996

			Winter (October–April)			All Year (January–December)			Summer (May–September)		
	Station	Latitude	Mean	SD	Samples	Mean	SD	Samples	Mean	SD	Samples
1	ALT	82°27′N	−27.13	1.02	28	−26.88	0.51	48	−27.09	0.71	20
2	ZEP	78°54′N	−25.65	1.51	17	−25.99	0.70	28	−26.87	1.01	11
3	MBC	76°15′N	−27.44	1.03	26	−26.93	0.50	46	−26.59	0.70	20
4	BRW	71°19′N	−26.19	1.10	28	−26.10	0.48	48	−26.00	0.64	20
5	STM	66°00′N	−25.12	1.63	17	−25.76	0.77	27	−26.42	1.13	10
6	ICE	63°15′N	−26.10	1.26	24	−26.59	0.56	44	−26.88	0.80	20
7	BAL	55°30′N	−26.33	1.11	23	−26.12	0.47	40	−28.74	1.11	17
8	CBA	55°12′N	−27.55	1.30	28	−27.69	0.51	48	−28.66	0.72	20
9	MHD	53°20′N	−25.82	1.23	28	−26.97	0.58	48	−27.38	0.87	20
10	SHM	52°43′N	−25.27	1.38	28	−26.92	0.49	48	−27.34	0.67	20
All stations combined			−26.3	0.4	247	−26.7	0.2	425	−27.1	0.3	178

stations used to construct the combined time series varied between 6 and 10. We did not perform any interpolation to account for missing data at individual stations. In the averaging process each station was weighted equally. Overall, the records from individual stations were mostly complete during the 1993–1996 period. In sum, 425 monthly mean data values were used to construct this combined time series (a perfect record without any missing monthly mean data would have contained 480 points for the 4-year interval). Standard deviation estimates for the combined time series reflected station to station differences in CO_2 and $\delta^{13}C$.

2.4. Atmosphere Model Description

[16] Pulse-response (or Green's) functions of the Goddard Institute for Space Studies (GISS) tracer model were used to construct a simple representation of a mean atmosphere with 16 "basis" surface regions (eight land and eight ocean) and a monthly time step (Table 3). The GISS tracer model uses 4-hour winds and monthly convection statistics from the GISS general circulation model and operates with a 1-hour time step [*Fung et al.*, 1991]. The pulse response functions were generated by evenly distributing a 1-Pg C source at the surface in each basis region for each month of the year and then recording the resulting three-dimensional (3-D) distribution (8° × 10° × 9 vertical layers) of CO_2 over a period of 3 years. On land the monthly pulse sources were distributed spatially within each basis region according to the annual mean distribution of NPP derived from the Carnegie-Ames-Stanford approach (CASA) model [*Randerson et al.*, 1997]. Ocean pulse sources were distributed evenly over the area of each ocean basis region (Table 3). Fossil fuel emissions were estimated using a single separate basis region with a spatial distribution described in section 2.8.

[17] In each land basis region a terrestrial biosphere model (described in section 2.5) was used to estimate ^{13}C and ^{12}C fluxes for each monthly time step. The terrestrial biosphere and atmospheric models were fully coupled in that surface fluxes from one land basis region in one time step would influence the isotopic composition of the atmosphere and consequently would influence the magnitude of isotopic exchange in terrestrial basis regions in future time steps. Because the coupling occurred at a monthly time step and terrestrial ecosystem isotope uptake occurred relative to the isotopic composition of the atmosphere at month $t - 1$, it is likely that the model somewhat underestimated the effects of seasonal changes in atmospheric $\delta^{13}C$ on the isotopic composition of ecosystem biomass and fluxes. In contrast to the terrestrial biosphere-atmosphere coupling, ocean and fossil fuel isotope fluxes were prescribed for the duration of each atmospheric model run using data sources described below.

[18] Within each land basis region the terrestrial biosphere model was 1-D; its input data and output fluxes did not vary spatially. Driver data (e.g., temperature or absorbed photosynthetically active radiation (APAR)) for the terrestrial model consisted of a single average value for each basis region, obtained by averaging data products with a higher spatial resolution. At each time step, atmospheric CO_2 concentrations resulting from terrestrial biosphere, ocean, and fossil fuel fluxes were added together using the appropriate pulse response functions for each. The procedure for estimating the atmospheric distribution of $\delta^{13}C$ was similar, as described below.

[19] In each pulse model simulation we carried two tracers, total carbon from the surface flux and the product of total carbon and the $\delta^{13}C$ isotopic signature of this flux in δ notation, i.e., $C \times \delta^{13}C$. The distribution of $\delta^{13}C$ in the

Table 3. Atmospheric Basis Regions

	Region	Location
	Land	
1	North America (high latitudes)	north of 56°N
2	Eurasia (high latitudes)	north of 56°N
3	North America (midlatitudes)	40°N–56°N
4	Eurasia (midlatitudes)	40°N–56°N
5	North America (low latitudes)	24°N–40°N
6	Eurasia (low latitudes)	24°N–40°N
7	Subtropics and tropics (Northern Hemisphere)	0°–24°N
8	Southern Hemisphere land	0°–56°S
	Ocean	
9	North Atlantic (high latitudes)	north of 40°N
10	North of Pacific (high latitudes)	north of 40°N
11	North Atlantic (low latitudes)	0°–40°N
12	North Pacific (low latitudes)	0°–40°N
13	South Atlantic	0°–48°S
14	South Pacific	0°–48°S
15	Indian Ocean	16°N–48°S
16	Southern Ocean	south of 48°S

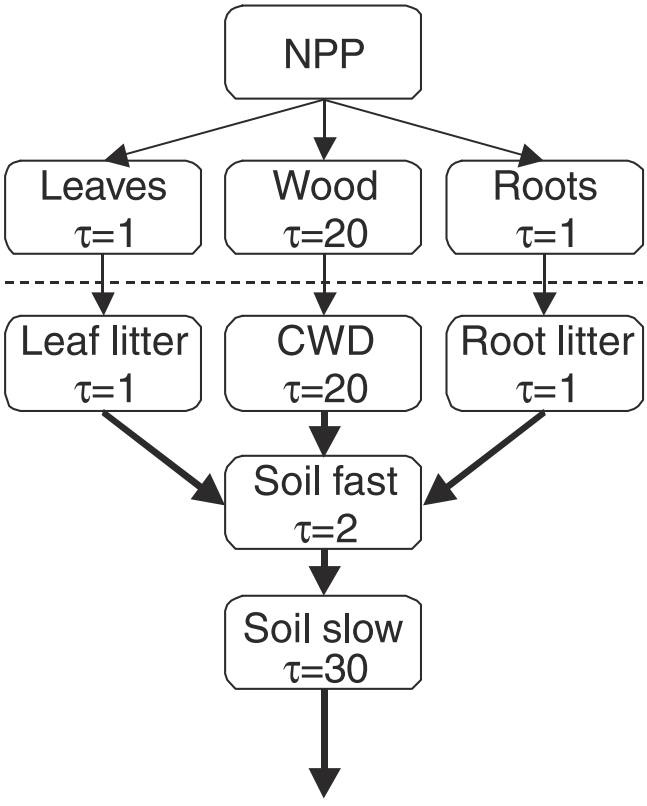

Figure 1. Diagram of carbon flow through the 8 pools in the 1-D terrestrial biosphere model employed in each terrestrial basis region. Transfers between pools below the dashed line were mediated by microbes with a transfer efficiency of 50% (i.e., 50% of each monthly flux was emitted to the atmosphere as heterotrophic respiration). Allocation of net primary production (NPP) to leaves, wood, and roots had the ratio 1:1:1. The turnover times of the various reservoirs in the model (i.e., equation (4) at 20°C were 1 year for leaves, roots, leaf litter, and root litter; 2 years for soil fast; 20 years for wood and coarse woody debris (CWD); and 30 years for soil slow.

atmosphere was then obtained by dividing the atmosphere distribution of $\delta^{13}CO_2 \times CO_2$ by the atmosphere distribution of CO_2 at the end of the simulation.

2.5. Terrestrial Biosphere Model Description

[20] We separately estimated monthly NPP and heterotrophic respiration (R_h) at each time step (t) and in each of the eight terrestrial basis regions (x). Monthly NPP was estimated as the product of APAR (in units of megajoules) and a light use efficiency (ε; in units of g C MJ^{-1} PAR) [*Montieth*, 1972]:

$$\mathrm{NPP}(x,t) = \mathrm{APAR}(x,t)\varepsilon. \tag{3}$$

APAR in equation (3) was estimated for each basis region by taking the average of 1° × 1° monthly maps generated by the CASA model. The CASA APAR estimates were derived from satellite-derived estimates of normalized difference vegetation index and total solar insolation [*Bishop and Rossow*, 1991; *Sellers et al.*, 1994; *Randerson et al.*, 1997]. The light use efficiency (ε) was uniform across all basis regions and time steps and, as described in section 2.9, is one of three "free" parameters solved for by comparison with atmospheric data.

[21] The heterotrophic respiration model had two components, a seasonal distribution and a time lag associated with the allocation of NPP to wood, fine roots, and leaves and then the decomposition of coarse woody debris, fine root litter, leaf litter, and fast and slow soil organic matter components (Figure 1). The seasonal distribution of R_h had a Q10 temperature dependence

$$\mathrm{R_h}(x,t) = \sum_{i=1}^{5} k(i)C(i,x,t)\ \mathrm{Q10}^{\frac{(T(x,t)-20)}{10}}, \tag{4}$$

where $k(i)$ is the decomposition rate constant for each pool i, C is the temporally and spatially (from basis region to basis region) varying carbon content of each pool, and Q10 represents the nonlinear factor that relates R_h to mean monthly air temperature, T. Mean monthly air temperatures for each basis region, x, were constructed from the spatial average of a 0.5° × 0.5° monthly climatology [*Leemans and Cramer*, 1990]. For our initial focus on high northern latitude ecosystems, we did not explicitly include soil moisture limitation on NPP or R_h.

[22] NEP is approximated in our model each month as the difference between NPP and R_h (Figure 2).

$$\mathrm{NEP}(x,t) \cong \mathrm{NPP}(x,t) - \mathrm{R_h}(x,t). \tag{5}$$

We make the additional approximation that this flux is entirely in the form of biosphere-atmosphere CO_2 exchange. While a formal definition of NEP includes any lateral, river, or biosphere-atmosphere flux of C that influences the net carbon balance of an ecosystem, our analysis focused on

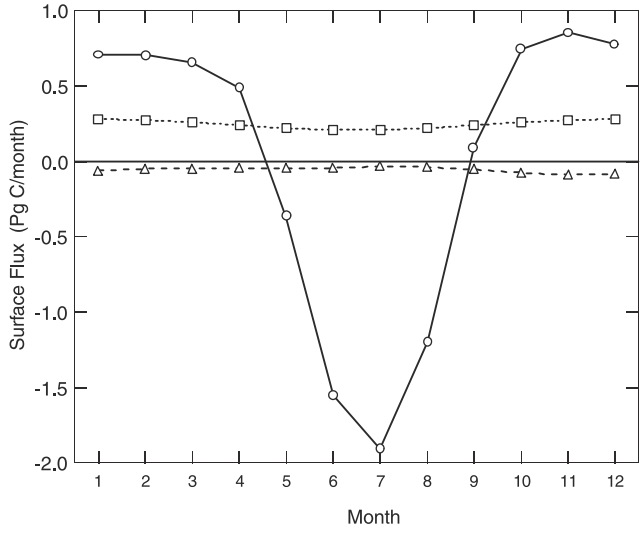

Figure 2. Monthly net ecosystem production (NEP) from the optimized terrestrial biosphere model for the sum of North America and Eurasia basis regions north of 40°N (solid line, circles), ocean exchange north of 40°N as described in the text (dashed line, triangles), and fossil fuel emissions north of 40°N (dotted line, squares).

seasonal timescales, and so this approximation is probably valid. It is worth noting, however, that fires are indistinguishable from R_h in our model formulation, and so they will impact on our inversion estimates of the Q10 temperature sensitivity and Δ_A^{13}, since they are a nonnegligible part of high-latitude seasonal CO_2 exchange [*French et al.*, 2000].

[23] Because of persistent fossil fuel CO_2 release of ^{13}C-depleted carbon, respiration of the terrestrial biosphere is not in equilibrium with the $\delta^{13}C$ content of the contemporary atmosphere (the $\delta^{13}C$ Suess effect [*Keeling et al.*, 1979]). The magnitude of the isotopic disequilibria depends on the residence time of C in vegetation, litter, and soils: The larger the mean residence time, the greater the isotopic disequilibria. Since the relative amounts of R_h and NPP in NEP vary from month to month, disequilibria effects have the potential to influence the isotopic composition of source estimated by equation (2). We accounted for disequilibria effects in each biosphere-atmosphere simulation by allowing the biosphere model to reach steady state with the atmosphere in the year 1750. Then, from 1750 to 1993 we used ice core and atmospheric $\delta^{13}C$ measurements from *Francey et al.* [1999] to adjust the ^{13}C of NPP and thus the ^{13}C content of model carbon pools. We tested our assumptions about the turnover time of carbon in the terrestrial biosphere with a sensitivity analysis described in section 2.9.

[24] We implicitly assumed that plant respiration was instantaneous (had a residence time that was less than the model time step of 1 month) and that there was no ^{13}C discrimination associated with this process. Because we attempted to separate and correct for isotopic disequilibria caused by time delays in R_h, our estimates of Δ_A^{13} represent a canopy-level discrimination associated with net photosynthetic assimilation [*Lloyd and Farquhar*, 1994]. It is not an ecosystem-level discrimination (Δ_E^{13}) that would include components from ecosystem respiration (as defined by *Buchmann et al.* [1998]).

2.6. Ocean Exchange

[25] Ocean exchange and its isotopic composition was estimated for each ocean basis region at each time step by separately considering the one-way gross fluxes:

$$^{13}F_{ao} \cong F_{ao} R_a \alpha_{ao} \quad (6a)$$

$$^{13}F_{oa} \cong F_{oa} R_o \alpha_{oa}. \quad (6b)$$

Equations (6a) and (6b) determine the flux of ^{13}C from the atmosphere to the ocean (ao) and from the ocean to the atmosphere (oa). The ^{13}C flux is determined by the total one-way flux, F, the $^{13}C/^{12}C$ ratio of the donor reservoir, R, and the fractionation factor associated with the flux, α. F_{ao} and F_{oa} were calculated from

$$F_{ao} = kpCO_{2\,atm} \quad (7a)$$

$$F_{oa} = kpCO_{2\,ocn}, \quad (7b)$$

where k is the gas transfer velocity and pCO_{2atm} and pCO_{2ocn} are the partial pressures of CO_2 in air and water, respectively [*Wanninkhof*, 1992]. The value of k was estimated from the *Wanninkhof* [1992] relationship for long-term averaged wind using the monthly mean wind climatology of *Esbensen and Kushnir* [1981]. The partial pressure of CO_2 in the ocean was derived from *Takahashi et al.* [1997].

[26] The $^{13}C/^{12}C$ ratio of the atmosphere, R_a, and pCO_{2atm} were estimated for the 1993–1996 period from the average of the atmospheric measurements listed in Table 1. For the ocean $^{13}C/^{12}C$ ratio, R_o, we used measurements of $\delta^{13}C$ in dissolved inorganic carbon (DIC) sampled from 1980 to 1995 as presented by *Gruber et al.* [1999]. The data were averaged over time and were linearly extrapolated to latitudinal bands in each ocean basin. The isotopic fractionation factors captured differences between DIC and gaseous CO_2 isotopic composition [*Zhang et al.*, 1995]. The temperature dependence of the fractionation factors [*Zhang et al.*, 1995] was calculated using monthly averaged simulated sea surface temperature from the National Center for Atmospheric Research Community Climate System Ocean Model [*Doney et al.*, 2001].

Table 4. Absorbed Photosynthetically Active Radiation and C3 and C4 Percent Net Primary Production

	Basis Region	APAR, MJ PAR $m^{-2}yr^{-1}$	C3, %	C4, %
1	North America north of 56°N	462.6	100	0
2	Eurasia north of 56°N	576.3	100	0
3	North America 40°N–56°N	926.6	99	1
4	Eurasia 40°N–56°N	456.0	100	0
5	North America 24°N–40°N	893.4	87	13
6	Eurasia 24°N–40°N	349.0	87	13
7	All land 0°N–24°N	1020.4	69	31
8	All land 0°S–56°S	957.2	78	22

2.7. C4 Vegetation

[27] We determined the contribution of C4 vegetation to the NPP flux in each land basis region using a new global map of C3 and C4 fractions [*Still et al.*, 2002]. The map was produced by combining physiological modeling and remote sensing products. The C4 component of NPP in each basis region (Table 4) was assigned a discrimination value of 4.4‰. We solved for the discrimination of the remaining C3 component of NPP (Δ_A^{13}) in the inversion analysis described in section 2.9.

2.8. Fossil Fuels

[28] We generated fossil fuel pulse functions using the GISS atmosphere model with a 1-Pg C source distributed spatially according to 1990 fossil fuel emissions [*Andres et al.*, 1996]. As with the terrestrial and ocean pulse functions, we constructed a separate pulse function for each month. However, in contrast to the ocean and terrestrial pulse functions, for fossil fuels we considered only a single spatial region, with the spatial distribution of fluxes prescribed by *Andres et al.* [1996]. For each year from 1990 to 1997, annual totals from *Marland et al.* [2000] were used to adjust the fossil pulse response functions to account for interannual variation. Seasonal variation in emissions was modeled using a sine wave with a peak in January, a minimum in July, and a peak-to-trough amplitude of 30%,

consistent with the seasonal distribution of consumption in North America and Europe [*Rotty*, 1987] (Figure 2). This probably had the effect of overestimating the seasonality of fossil fuel emissions in the tropics. However, fossil fuel emissions in the tropics are relatively small [*Andres et al.*, 1996]. Given that the focus of our study is on high northern latitudes and that detailed spatial data on seasonal emissions are sparse, it is difficult to justify a more elaborate representation of fossil emissions.

[29] To estimate the isotopic variations in Northern Hemisphere fossil fuel, we assumed that gas, solid, and liquid components of fossil fuel emissions were 20, 45, and 35%, respectively, based on 1990 data from North America, Western Europe, Germany, Centrally Planned Europe, Centrally Planned Asia, and Far East Asia [*Marland et al.*, 2000]. Gas, solid, and liquid fuels were assigned isotopic values of −42, −24, and −28‰, respectively [*Andres et al.*, 2000]. We used compiled, available records for the United States [*Rotty*, 1987] to describe seasonal variation in gas, solid, and liquid fuel use. The dominant contributor to seasonal variation in fossil fuel emissions was natural gas. Natural gas consumption in the United States doubled during winter months because of increased heating demands (from 6.4% in July to 13.3% in January) [*Rotty*, 1987].

2.9. Biosphere-Atmosphere Model Simulation

[30] The primary objective of the model simulations was to estimate the combination of Δ_A^{13}, ε, and Q10 parameters that best described the high-latitude NOAA/INSTAAR observations. We accomplished this sequentially with two steps. First, we solved for the combination of ε and Q10 that minimized the error between modeled and measured monthly CO_2 as described by the following cost function:

$$\Theta_1 = \sum_{j=1}^{48\ \text{months}} \left(\frac{C_{\text{obs}}(j) - C_{\text{mod}}(j)}{\sigma_{\text{obs}}(j)} \right)^2, \qquad (8)$$

where C_{obs} was the combined and detrended monthly time series of NOAA CO_2 described in section 2.3 (the average of the stations in Table 1 for each of the 48 monthly intervals between January 1993 and December 1996), C_{mod} was the combined and detrended CO_2 time series from the atmospheric model (consisting of the average of the surface grid cells containing the stations listed in Table 1), and $\sigma_{\text{obs}}(j)$ was the standard deviation of the observations across all available stations in each time step. Each estimate of C_{mod} included prescribed ocean and fossil fuel emissions as described in sections 2.6 and 2.8. We estimated Θ_1 for a series of terrestrial biosphere model scenarios (section 2.5) in which ε ranged between 0.1 and 0.9 g C MJ^{-1} PAR (at 0.01 g C MJ^{-1} PAR increments) and the Q10 simultaneously ranged between 1.0 and 2.2 (at 0.01 increments). Thus Θ_1 was computed for ~9600 terrestrial biosphere model scenarios. We report minimum values of ε and Q10 in section 3 along with the shape of the cost function. With the first step of this minimization process we were effectively searching for two free variables (ε and Q10), using a constraint of 48 mean monthly CO_2 observations from high northern latitude stations (section 2.3).

[31] Second, with the ε and Q10 that minimized equation (8), in a second series of model runs we varied Δ_A^{13} between 15 and 23‰ at 0.01‰ increments. The cost function for this second minimization step had the same form as equation (8), but for $\delta^{13}C$ instead of CO_2. With the second step of this minimization process we were effectively searching for one free variable (Δ_A^{13}) using a constraint of 48 mean monthly $\delta^{13}C$ observations from high northern latitude stations (section 2.3).

[32] We also used the monthly atmospheric distribution of $\delta^{13}C$ and CO_2 from each model run to calculate the modeled source composition, $\delta^{13}C_n$ (model), from equation (2). The combined model time series was constructed in an identical manner to the combined NOAA/INSTAAR time series, described in section 2.1 and 2.3, by averaging the $\delta^{13}C$ and CO_2 of surface grid cells that corresponded to the stations listed in Table 1. The Δ_A^{13} of the terrestrial biosphere that minimized the difference between observed and modeled $\delta^{13}C_n$ served as a second cost function, Θ_2.

$$\Theta_2 = \left| \delta^{13}C_n(\text{obs}) - \delta^{13}C_n(\text{model}) \right|. \qquad (9)$$

[33] Equation (9) serves as a useful alternate to equation (8) because it emphasizes different aspects of the NOAA and INSTAAR data record. Specifically, equation (9) (which is based on the modeled and observed intercepts from equation (2)) is relatively insensitive to biases in the shape of the modeled seasonal cycle that are present in both $\delta^{13}C$ and CO_2. Specifically, equation (9) depends more on the relationship between $\delta^{13}C$ and CO_2 (the slope and intercept in $\delta^{13}C$ and CO_2 phase space) than on the exact shape of the $\delta^{13}C$ seasonal cycle.

[34] We also used our atmospheric pulse model to estimate the atmospheric isotopic composition at the time of photosynthetic fixation ($\delta^{13}C_{atm}$). We estimated ($\delta^{13}C_{atm}$) by weighting monthly surface-level atmospheric $\delta^{13}C$ values over the continents north of 40°N (over basis regions 1, 2, 3, and 4 in Table 3) by monthly APAR from the same regions (described in section 2.5).

[35] In the following results section, we separately provide the distribution of the error function for the two steps in our inversion procedure. Formal estimates of the errors are difficult to retrieve because of bias introduced from the use of modeled atmospheric winds.

[36] In a series of sensitivity tests, we report the optimal Δ_A^{13} of the terrestrial biosphere (minimum of equation (9)) when ocean, fossil fuel, and remote C4 fluxes were sequentially removed from the model calculation of CO_2 and $\delta^{13}C$. We also conducted sensitivity analyses in which the mean residence time of each pool in the terrestrial biosphere model (shown in Figure 1) was divided by a factor of 2.

3. Results

3.1. The Isotopic Composition of Net Seasonal CO_2 Exchange

[37] Using all available mean monthly data north of 50°N from January 1993 through December 1996, we find that the isotopic composition of net seasonal CO_2 exchange, $\delta^{13}C_n$, was −26.7‰ ± 0.2‰ (Table 2). The $\delta^{13}C_n$ varied between winter and summer: wintertime flask data (Octo-

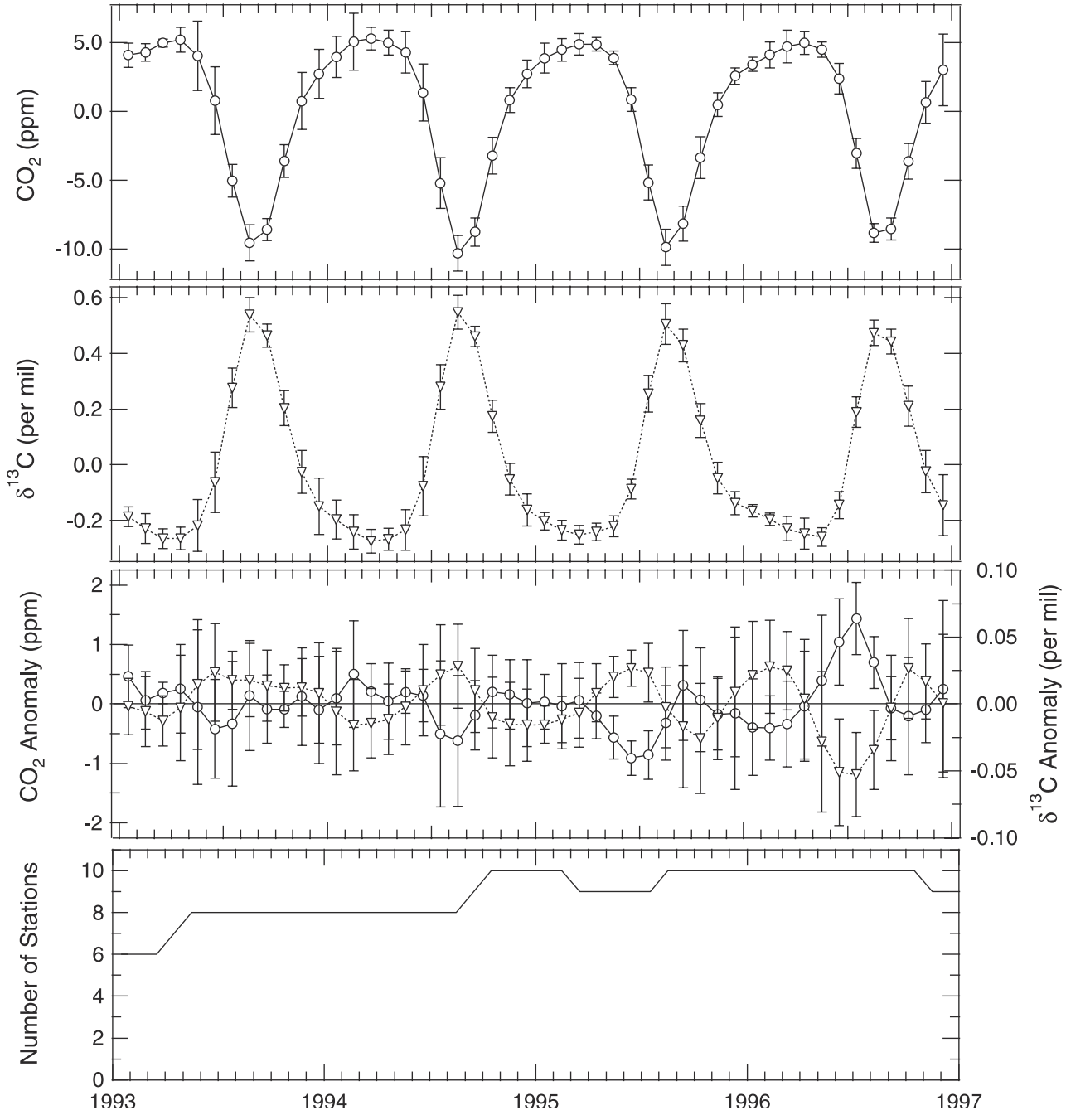

Figure 3. The detrended, combined time series (section 2.3) from January 1993 to December 1996 used to retrieve $\Delta_A{}^{13}$, ε, and Q10 biosphere parameters. (a) Monthly CO_2. (b) Monthly $\delta^{13}C$. (c) Monthly anomalies in CO_2 (left axis) and $\delta^{13}C$ (right axis), obtained by removing a mean seasonal cycle. (d) Number of individual stations from Table 1 that contributed to each monthly interval.

ber–April) yielded a $\delta^{13}C_n$ of −26.3‰ ± 0.4‰, while summertime flask data (May–September) yielded a $\delta^{13}C_n$ of −27.1 ± 0.3‰ (Table 2).

[38] Monthly and seasonal anomalies in CO_2 and $\delta^{13}C$ from the stations in Table 1 were coherent across widely distributed and remote northern observation sites (Figure 3). May, June, and July of 1995 had anomalously low CO_2 and anomalously high $\delta^{13}C$. In contrast, during the growing season in 1996, CO_2 was anomalously high, and $\delta^{13}C$ was anomalously low (Figure 3c). The CO_2 and $\delta^{13}C$ anomalies had a highly significant negative Pearson correlation ($r = -0.84$, $df = 46$, and $p < 0.01$). A linear regression of the anomalies in $\delta^{13}C$ and CO_2 (equation (2)) yielded a source isotopic composition of −22.9‰ ± 4.6‰. The anomalies may reflect, in part, interannual changes in Δ_A^{13}. The relatively low isotopic source value of the CO_2 anoma-

Table 5. Sensitivity Analysis of ε Q10, and Δ_A^{13} Retrievals[a]

	Fluxes Included in Simulation	Description	ε, gC MJ^{-1} PAR	Q10	MRT Regions 1 and 2, years	MRT Region 7, years	Global NPP, Pg C/yr	$\delta^{13}C$ Global Disequilibria, Pg C ‰/yr	Δ_A^{13}, ‰
1.	FF + ocean + remote C4 + land model	standard run	0.47	1.52	42	18	55	22.7	19.0
2.	ocean + C4 + land model	no fossil	0.51	1.53	42	17	60	24.7	19.2
3.	FF + C4 + land model	no ocean	0.45	1.48	41	18	53	21.7	18.9
4.	FF + ocean + land model	no C4	0.47	1.52	42	18	55	22.7	19.0
5.	FF + ocean + C4 + modified land model with τ_i/2.0	MRT[b]/2	0.47	1.52	22	9	55	15.6	19.1

[a] For each of the four sensitivity model runs (runs 2–5) the surface fluxes used in the inversion analysis were modified either by removing the fossil fuel (FF) source, removing the ocean source, removing the influence of C4 vegetation, or modifying carbon pools within the terrestrial biosphere model. The Δ_A^{13} values are reported using equation (9) for the minimization function.

[b] Mean residence time (MRT) of all terrestrial biosphere model carbon pools were decreased by a factor of 2 from those shown in Figure 1. This had the effect of changing the isotopic disequilibria and the isotopic composition of heterotrophic respiration.

lies (−22.9‰), however, may also reflect a nonnegligible contribution to interannual variability from high-latitude air-sea gas exchange, biomass burning, or changes in the isotopic composition of fossil emissions.

3.2. Biosphere-Atmosphere Model Results

[39] The ε and Q10 values that simultaneously minimized error between modeled and NOAA/CMDL CO_2 observations were 0.47 g C MJ^{-1} PAR and 1.52 (Table 5). The optimized ε value generated a mean North American NPP of 217 g C m^{-2} yr^{-1} north of 56°N, a mean Eurasian NPP of 271 g C m^{-2} yr^{-1} north of 56°N, and a global total of 55 Pg C yr^{-1}. The optimized Q10 value generated a mean residence of terrestrial carbon of 42 years for North American and Eurasian regions north of 56°N (basis regions 1 and 2), a mean residence time for tropical and subtropical regions of the Northern Hemisphere of 18 years (basis region 7), and a global mean residence time of 24 years (given the structure of the biosphere model described in the text and in Figure 1).

[40] These results demonstrate that the Q10 function also partially constrains the latitudinal distribution of ecosystem carbon turnover times and thus constrains the latitude distribution of the isotopic disequilibria of R_h, a critical parameter in regional and global scale double deconvolution estimates of ocean and land carbon sinks [*Ciais et al.*, 1995]. With an optimized Q10 of 1.52, the global isotopic disequilibria forcing at the start of our simulations in 1990 was 22.7 Pg C ‰ yr^{-1}.

[41] More generally, the combinations of ε and Q10 that minimized error (equation (8)) were correlated because these two parameters together determined the seasonal distribution of the net land flux (Figure 4). The ε sets the magnitude of NPP, since the distribution of APAR was fixed from satellite observations (section 2.5). The Q10 set the seasonal distribution of R_h based on monthly air temperatures (equation (4)). In northern biomes a higher Q10 leads to a higher fraction of R_h emitted during summer months than during winter months. For the ecosystem to sustain a net carbon sink during the summer (required to match the observations in Figure 3a), ε must also be high, so that NPP exceeds R_h [*Lloyd and Taylor*, 1994].

[42] The value of Δ_A^{13} that minimized the difference in the observed and modeled source composition was 19.4‰ (equation (8) and Figure 5). Use of an alternate cost function led to an Δ_A^{13} estimate of 19.0‰ (equation (9)).

[43] From our sensitivity analysis, retrieval of Δ_A^{13} from atmospheric data appeared most sensitive to fossil fuel emissions. Excluding fossil fuel fluxes from the analysis led to an increase in Δ_A^{13} by 0.2‰, while excluding ocean exchange led to a decrease of Δ_A^{13} by 0.1‰ (Table 5). Excluding remote C4 ecosystems also caused a decrease of

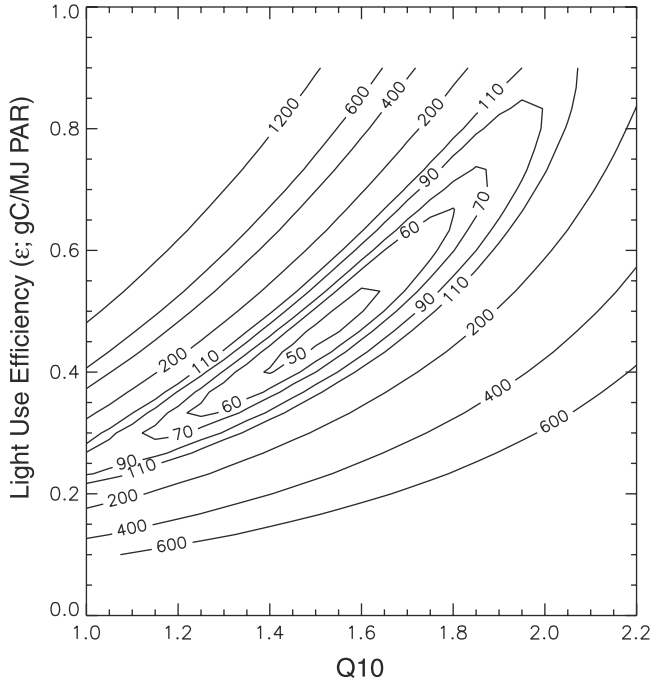

Figure 4. Cost function space for ε and Q10 parameters that best match the NOAA/CMDL CO_2 data. Contour intervals denote levels of the cost function defined by equation (8). A Q10 of 1.52 and an ε of 0.47 g C MJ^{-1} PAR minimized the cost function.

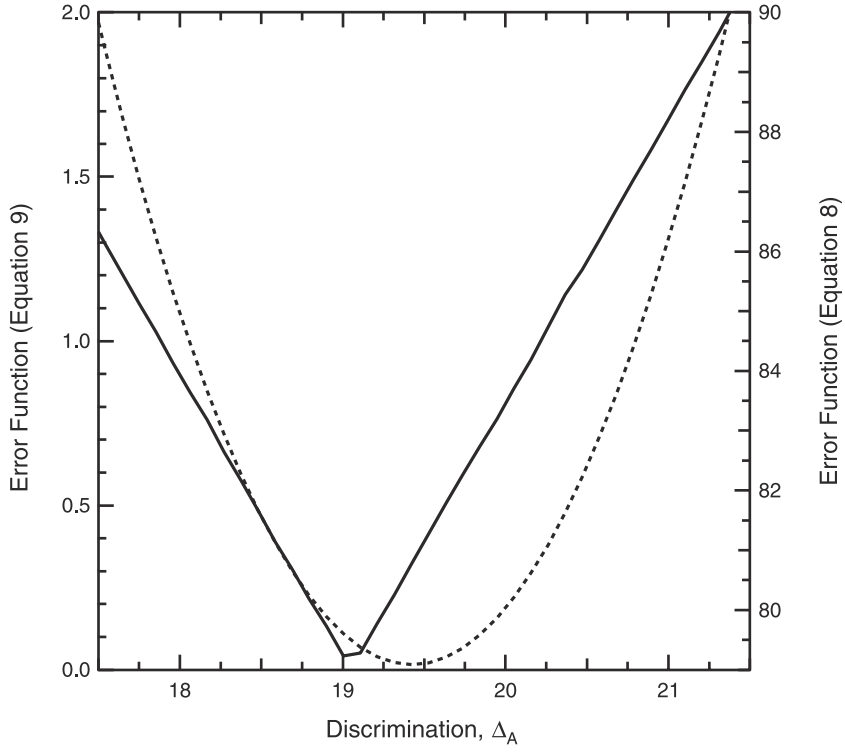

Figure 5. The two cost functions from the atmospheric inversion procedure for Δ_A^{13} are presented. Equation (8) is given by the dashed line and corresponds to the right axis. Equation (9) is given by the solid line and corresponds to the left axis. The Δ_A^{13} values of 19.4 and 19.05‰ minimized equations (8) and (9), respectively.

Δ_A^{13} (oceans and C4 fluxes have a similar impact on Δ_A^{13}), but for the northern regions that were the focus of this analysis, the effect was <0.05‰. Cutting the turnover time of each terrestrial biosphere model carbon pool in half caused the isotopic disequilibria forcing to decrease by $\sim$7 Pg C‰ yr^{-1} and caused Δ_A^{13} to increase by 0.1‰.

[44] With the Δ_A^{13}, ε, and Q10 values that minimized the cost functions, the model does a fair job at reproducing the mean seasonal cycle at high northern latitude observation stations, although during the early part of the growing season the model drawdown of CO_2 occurs earlier than in the observations (Figure 6). Over the continents the seasonal cycle of $\delta^{13}C_{atm}$ is even greater than at the observation stations (Figure 6c). For example, over land north of 56°N, $\delta^{13}C_{atm}$ increases by $\sim$1.0‰ from May to September. Over land between 40°N and 56°N, $\delta^{13}C_{atm}$ increases by $\sim$0.8‰ from May to September. For grid cells in the middle of the continents, this seasonal variation is even larger (data not shown). When monthly $\delta^{13}C_{atm}$ values over continental regions north of 40°N were averaged over the growing season (weighted according to monthly APAR), we obtained a value of $-$8.0‰.

4. Discussion

4.1. Δ_A^{13} for Northern Biomes

[45] Two lines of evidence suggest that Δ_A^{13} for northern biomes, integrated over the growing season, is between 19.0 and 19.6‰. The first is the analysis of high northern latitude CMDL and INSTAAR data that documents a more negative source during summer months ($-$27.1‰) than during winter months ($-$26.3‰). During the summer, fluxes from ocean and fossil fuels are small relative to fluxes from the terrestrial biosphere (Figure 2). To a first approximation, during summer months it may be possible to ignore monthly variations arising from fossil fuel and ocean exchange, whereas during the winter this would be impossible. With a mean summer source composition of -27.1 ± 0.3‰ and an APAR-weighted atmospheric composition over northern continents of $-$8.0‰ from 1993 to 1996 (section 2.9), it is possible to directly estimate a value of Δ_A^{13} at $\sim$19.6‰ without use of an atmospheric inversion.

[46] Can fossil fuel emissions be neglected during summer? In this context, it is crucial to note that only the seasonally varying component of fossil fuel emissions induces a bias in a direct estimate of Δ_A^{13}. The seasonally invariant component of the fossil fuel flux (which constitutes most of the fossil flux; see Figure 2) is mostly removed from the NOAA and INSTAAR data prior to our analysis by the application of the low-frequency smoothing spline (section 2.1). For the same reason, only the seasonally varying component of the ocean exchange would induce a bias. More generally, with any analysis of regional aircraft or surface measurements the distinction between background and seasonally varying contaminants must be addressed prior to correcting for their effects with a mixing

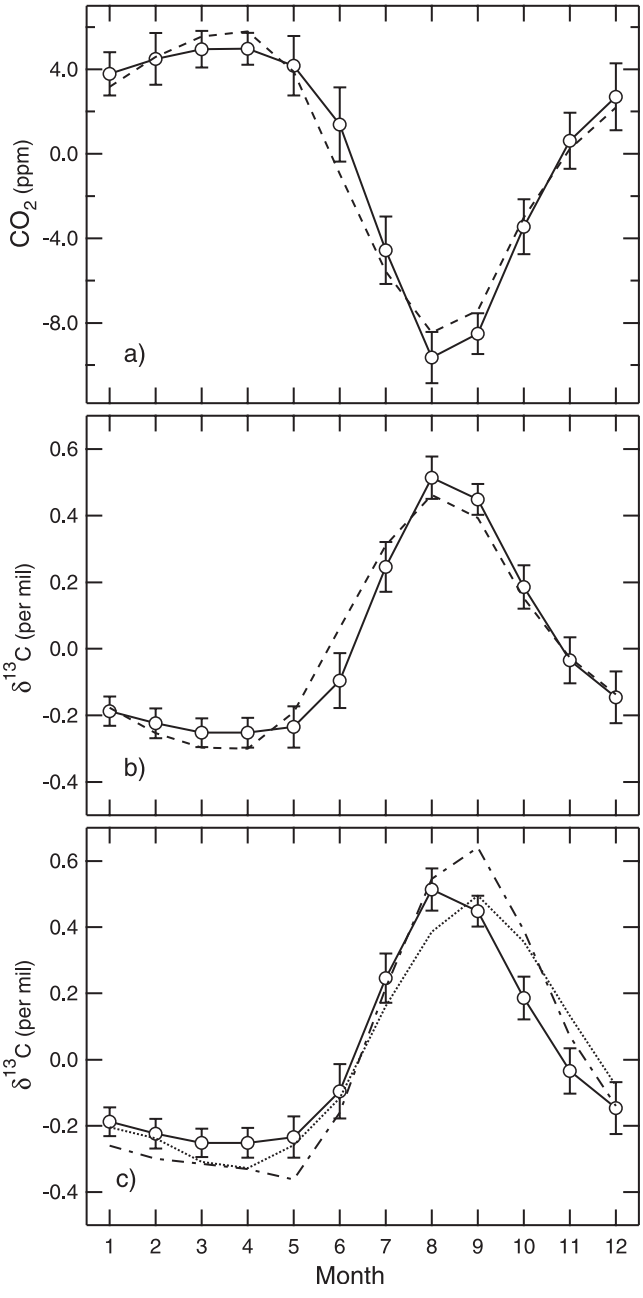

Figure 6. (a) Modeled CO_2 concentration (dashed line) from the grid cells that cover the high-latitude NOAA/CMDL observation sites listed in Table 1 using optimized ε and Q10 values. (b) Same as in Figure 6a but for $\delta^{13}C$ with Δ_A^{13} optimized from equation (9). (c) Modeled seasonal cycle averaged over all land area between 40°N and 56°N (dotted line) and over all land area north of 56°N (dash-dotted line). Observations (see section 2.3) are represented by the solid line and standard deviation error bars.

model approach. This is particularly challenging when CO is used to correct for fossil fuel contamination; only the seasonally varying component of CO is appropriate for fossil fuel corrections on seasonal timescales, and variation arising from reaction with atmospheric OH or biomass burning sources must be separately accounted for [*Bakwin et al.*, 1998].

[47] The second line of evidence for Δ_A^{13} being $\geq$19.0‰ comes from our full biosphere-atmosphere inversion analysis that includes seasonal variation in atmospheric transport, and it accounts for the seasonal distribution of fossil fuel, ocean, and remote C4 ecosystem contributions. Given that the minima of two cost functions differ by ~0.4‰ (minima of 19.4 and 19.0‰ for equations (8) and (9), respectively), that the standard error of the observed $\delta^{13}C_n$ is at least 0.2‰ (Table 2), and that the range from sensitivity analysis is 0.3‰ (Table 3), it is difficult to ascribe a confidence level to Δ_A^{13} of less than ±1.0‰. Precise estimates of uncertainty are limited with the inversion techniques because of the difficulty in quantifying biases introduced from atmospheric transport. Nevertheless, the sharp increase in the cost functions below 18.0‰ and above 21.0‰ and our sensitivity analysis allow us to effectively bracket the high-latitude flux-weighted value. Our Δ_A^{13} estimate is slightly less than the mean of respiration estimates from boreal ecosystems in central Canada [*Flanagan et al.*, 1996] and is comparable with estimates inferred directly from high northern latitude aircraft observations in the lower [*Nakazawa et al.*, 1997] and upper troposphere [*Zahn et al.*, 2000].

[48] Other atmospheric models may generate stronger land/ocean CO_2 gradients during the growing season. If the atmosphere was more enriched over land during summer months than we were able to produce with our monthly pulse model (Figure 6), Δ_A^{13} may be even larger than our inversion model suggests. Also, with our atmospheric pulse model we were unable to capture any covariance between diurnal variations in the atmospheric isotopic composition over land and diurnal patterns of CO_2 fixation. Failing to capture this covariance may impose an offset in our inversion estimates of Δ_A^{13} to the extent that fixation occurs at times when CO_2 in the boundary layer deviates significantly from background troposphere concentrations. Failing to capture this diurnal process would most likely cause us to underestimate Δ_A^{13} in our inversion.

[49] Boreal forest and arctic tundra biomes are the greatest contributors to seasonal variation in CO_2 at the stations listed in Table 1 [*Kaminski et al.*, 1996; *Randerson et al.*, 1997], and so the Δ_A^{13} estimate we obtain from our inversion mostly reflects a flux-weighted average of C3 vegetation in these two biomes. Since fluxes from nonvascular plants such as mosses and lichens have a significant role in modulating atmospheric CO_2 in the far north on seasonal timescales, these fluxes also contribute to our estimate of Δ_A^{13}. Mosses may account for 10–40% of boreal forest and wetland NPP [*Frolking*, 1997; *Szumigalski and Bayley*, 1996] and have an isotopic composition that often is depleted by several per mil as compared with conifer trees growing at the same sites [*Brooks et al.*, 1997; *Flanagan et al.*, 1997]. Some of this depletion is caused by elevated levels of atmospheric CO_2, near the forest floor, from soil respiration.

[50] The contribution of fluxes from mosses and lichens at high northern latitudes makes it difficult to compare our biome-level inversion estimates with models that focus

exclusively on vascular plants with stomatal regulation [*Lloyd and Farquhar*, 1994]. Similarly, the dominance of conifers in many regions makes it difficult to directly compare our estimates with syntheses that focus solely on herbaceous plants [*Korner et al.*, 1991].

[51] The top-down inversion estimate of Δ_A^{13} presented here may allow us to place a constraint on the relative contribution of various plant functional types to the total seasonal CO_2 exchange at high northern latitudes. Evergreen conifers tend to have lower Δ_A^{13} values ($\sim$18.5 $\pm$ 1.0‰) than deciduous (larch) conifers ($\sim$19.5 $\pm$ 1.0‰) [*Kloeppel et al.*, 1998], while deciduous trees, shrubs, and mosses appear to have Δ_A^{13} values that frequently exceed 20‰ ($\sim$21–23‰) [*Brooks et al.*, 1997; *Flanagan et al.*, 1997]. Consequently, our biome-level estimate of 19.0–19.6‰ suggests that deciduous trees, shrubs, and mosses have an important but limited role in shaping the total seasonal flux in northern biomes.

[52] Several previous analyses of Δ_A^{13} at the ecosystem scale have assumed that $\delta^{13}C_{atm}$ was constant over the duration of the growing season. We find that $\delta^{13}C_{atm}$ increases by up to 1.0‰ from May to September over northern land regions. This offset has implications for ecosystem-level Δ_A^{13} analyses in that different species/plant functional types may take up carbon over different periods within the growing season. This seasonal trend in $\delta^{13}C_{atm}$ is consistent with observations from central Canada [*Flanagan et al.*, 1997] and is larger than the seasonality observed at remote, marine NOAA/CMDL and INSTAAR flask observation stations that are frequently invoked as a reference for ecosystem-level studies.

4.2. Light Use Efficiency

[53] Three kinds of approaches exist for estimating ε at regional and biome scales, two that depend on NPP measurements and a third that depends on an atmospheric inversion of the net flux (this study, *Kaminski et al.* [2002], and *Knorr and Heimann* [1995]). The NPP-based methods can be categorized as those that extrapolate in situ ε observations using vegetation or biome type [*Heimann et al.*, 1989; *Ruimy et al.*, 1994] and those that use a dynamic model of ε that responds to variation in climate [*Running and Hunt*, 1993; *Runyon and Waring*, 1994; *Field et al.*, 1995]. Development and application of the NPP-based methods requires, as a minimum, precise NPP observations at a series of sites that span the observed range of environmental variability.

[54] The top-down atmospheric inversion approach for estimating ε is complementary to the NPP-based methods in that NPP observations are not required. The tradeoff is that additional constraints must come from models of R_h, APAR, and atmospheric transport and from very precise atmospheric trace gas measurements. On seasonal timescales in middle- and high-latitude regions of the Northern Hemisphere, these constraints are relatively well defined. Heterotrophic respiration is highly sensitive to temperature, and a number of studies have defined the form of this relationship [*Lloyd and Taylor*, 1994; *Raich and Potter*, 1995]. In the tropics, additional challenges arise in applying the inversion approach from relatively small CO_2 gradients (from rapid tropical convective mixing), greater contribution of ocean exchange, uncertainties in our understanding of the relationship between soil moisture limitation, respiration, and NEP, and differing light use efficiencies of C4 plants.

[55] Given the limitations of the inversion approach described above, our estimate of a NPP-based ε of 0.47 gC MJ^{-1} PAR for boreal and arctic biomes is greater than observations from boreal and temperate evergreen conifer forests ($\sim$0.3 gC MJ^{-1} PAR) but less than or comparable with boreal deciduous (aspen) and temperate deciduous (mixed hardwood) observations ($\sim$0.5 gC MJ^{-1} PAR) [*Gower et al.*, 1999]. Since the cost function does not rise sharply when ε and Q10 values covary, it is possible to match the observed values of ε in boreal conifers by accepting a series of slightly less ideal solutions with smaller Q10 values (Figure 4). Biases in our estimates of ε may also arise from any systematic offset in our satellite-derived APAR estimates (presented in Table 4).

[56] Compared with dynamic ε models, the inversion value we obtain is $\sim$20% greater than the CASA globally maximum ε value (0.39 gC MJ^{-1} PAR) that was obtained from a set of worldwide NPP measurements [*Field et al.*, 1995]. Part of this difference may be attributed to a greater fraction of diffuse light at high northern latitudes, which would increase an atmospheric inversion-based estimate of ε as compared to the CASA analysis that relied on global NPP observations, and did not involve a partitioning of PAR into diffuse or direct components.

[57] In principal, the inversion approach presented here could be extended to estimate gross primary product based light use efficiencies. A model of plant maintenance and growth respiration would be required, along with a model that described the age distribution of plant respiration. Including plant respiration would probably require a biosphere-atmosphere model that operated with a shorter time step.

4.3. Use of the Q10 Function in Biogeochemical Models

[58] We used mean monthly temperature data to obtain a Q10 of 1.52. This Q10 value is appropriate for use with ecosystem NPP models that operate with a monthly time step, predict respiration fluxes using air temperature, and are used to predict seasonal to interannual dynamics in heterotrophic respiration.

[59] Our biome-level estimate falls in the middle of a 1.4–1.6 range of Q10 values reported from a metaanalysis of soil respiration data that were analyzed with respect to mean monthly air temperatures [*Raich and Potter*, 1995] and is consistent with other atmospheric inversions that relate respiration fluxes to monthly air temperatures [*Kaminski et al.*, 2002; *Knorr and Heimann*, 1995]. Together, the atmospheric inversion results and the soil respiration syntheses challenge the idea that a single canonical Q10 value of 2 is appropriate for relating ecosystem responses to temperature and reinforce the idea that Q10 values must be specifically defined for a given time and space scale of temperature variability.

[60] The top-down estimate of the Q10 is much lower than estimates obtained from the comparison of soil respi-

ration fluxes with soil temperatures (median Q10 of 2.4 [*Raich and Schlesinger*, 1992]). The reason for this stems from physical, physiological, and ecological limits on scaling respiration estimates. If we had used soil temperatures instead of air temperatures to drive our respiration model, the Q10 value that minimized the error function would have increased for any given value of ε, because soil temperatures have a damped seasonal cycle as compared with air temperatures [*Ryan*, 1991].

[61] Another critical factor that must be accounted for in the Q10 formulation is that the pool of metabolically active carbon in plant biomass and soil changes seasonally because of increases in living plant biomass over the growing season and, in the far north, because of soil thaw and an extension of the active layer through the summer and into the fall. This process is only partially captured with our model formulation; biomass pools do change seasonally, but soil depth does not. In addition, fires in the boreal forest contribute to some of the interannual variability in atmospheric CO_2 shown in Figure 3 [*French et al.*, 2000]. In our analysis, we do not explicitly correct for the fire fluxes (which occur exclusively during summer months), and so we may overestimate the sensitivity of heterotrophic respiration to temperature.

4.4. Improving Future Estimates of Δ_A^{13}

[62] Knowledge of the magnitude and isotopic composition of monthly fossil fuel emissions limits our ability to retrieve more precise estimates of Δ_A^{13} in northern ecosystems using the inverse atmospheric approach. In our sensitivity analysis, removal of the fossil fuel source led to the largest perturbation of our Δ_A^{13} estimate (0.2‰; see Table 5). In the far north it is not clear if fossil emissions increase or decrease during the summer; there is greater demand for heating during winter months, yet there is greater economic activity during the summer. With the development and application of higher resolution atmospheric models the impact of fossil fuels on inversion results is likely to be even greater, particularly for continental regions like the United States that have high fossil emissions. Natural gas is a primary source of this limitation, because its isotopic composition varies widely and its use may vary substantially from summer to winter and also, possibly, from year to year. More detailed information on monthly fossil fuel emissions is also essential for inversion analyses that retrieve seasonally varying sources and sinks of CO_2, particularly with the double deconvolution approach [*Ciais et al.*, 1995], but also for the case of time-dependent CO_2 inversions [*Rayner et al.*, 1999].

5. Conclusions

[63] Here we provide top-down estimates of three ecophysiological parameters for northern tundra and boreal forest biomes. We find that Δ_A^{13} is $\sim$19.0–19.6‰, ε is $\sim$0.47 gC MJ^{-1} PAR, and the Q10 is $\sim$1.52. On land these three ecophysiological parameters may be among the easiest to retrieve from remote atmospheric observations. Ultimately, developing top-down estimates of biospheric parameters provides additional dimensions (beyond flux estimates) to test our understanding of ecosystem function across multiple time and space scales. For example, changes in disturbance regime in the boreal forest will alter fluxes, but it will also alter Δ_A^{13} in a way that is predictable and is possibly detectable over a period of several decades.

[64] With longer time series of precise CO_2 and $\delta^{13}C$ measurements, it may be possible to identify seasonal variation in Δ_A^{13} and magnitude of ecosystem isotopic disequilibria, taking advantage of the subtle month-to-month variations in $\delta^{13}C$-CO_2 phase space. In principle, it should also be possible to solve for discrimination from all land and ocean regions, following the time-dependent methodology developed by *Rayner et al.* [1999] and *Bousquet et al.* [2000] for atmosphere CO_2. If land and ocean fluxes at the same latitude are truly distinguishable with surface flask data, then a $\delta^{13}C$ inversion should yield ocean and land discrimination values that are consistent with direct observation.

[65] **Acknowledgments.** J. T. R. gratefully acknowledges support from a NASA IDS grant NASA/MDAR NAG5-9462 and a DOE Alexander Hollaender Distinguished Postdoctoral Fellowship.

References

Andres, R. J., G. Marland, I. Y. Fung, and E. Matthews, A 1° × 1° distribution of carbon dioxide emissions from fossil fuel consumption and cement manufacture, 1950–1990, *Global Biogeochem. Cycles*, *10*(3), 419–430, 1996.

Andres, R. J., G. Marland, T. Boden, and S. Bischof, Carbon dioxide emissions from fossil fuel consumption and cement manufacture, 1751-1991, and an estimate of their isotopic composition and latitudinal distribution, in *The Carbon Cycle*, edited by T. M. L. Wigley and D. S. Schimel, pp. 53–62, Cambridge Univ. Press, New York, 2000.

Bakwin, P. S., P. P. Tans, J. W. C. White, and R. J. Andres, Determination of the isotopic (C-13/C-12) discrimination by terrestrial biology from a global network of observations, *Global Biogeochem. Cycles*, *12*(3), 555–562, 1998.

Battle, M., M. L. Bender, P. P. Tans, J. W. C. White, J. T. Ellis, T. Conway, and R. J. Francey, Global carbon sinks and their variability inferred from atmospheric O_2 and $\delta^{13}C$, *Science*, *287*(5462), 2467–2470, 2000.

Benner, R., M. L. Fogel, E. K. Sprague, and R. E. Hodson, Depletion of C-13 in lignin and its implications for stable carbon isotope studies, *Nature*, *329*, 708–710, 1987.

Bird, M. I., and P. Pousai, Variations of $\delta^{13}C$ in the surface soil organic carbon pool, *Global Biogeochem. Cycles*, *11*(3), 313–322, 1997.

Bird, M. I., A. R. Chivas, and J. Head, A latitude gradient in carbon turnover times in forest soils, *Nature*, *381*, 143–145, 1996.

Bishop, J. K. B., and W. B. Rossow, Spatial and temporal variability of global surface solar irradiance, *J. Geophys. Res.*, *96*(C9), 16,839–16,858, 1991.

Bousquet, P., P. Peylin, P. Ciais, C. Le Quere, P. Friedlingstein, and P. P. Tans, Regional changes in carbon dioxide fluxes of land and oceans since 1980, *Science*, *290*(5495), 1342–1346, 2000.

Bowling, D. R., D. D. Baldocchi, and R. K. Monson, Dynamics of isotopic exchange of carbon dioxide in a Tennessee deciduous forest, *Global Biogeochem. Cycles*, *13*(4), 903–922, 1999.

Bowling, D. R., N. G. McDowell, B. J. Bond, B. E. Law, and J. R. Ehleringer, ^{13}C content of ecosystem respiration is linked to precipitation and vapor pressure deficit, *Oecologia*, in press, 2002.

Brooks, J. R., L. B. Flanagan, N. Buchmann, and J. R. Ehleringer, Carbon isotope composition of boreal plants: Functional grouping of life forms, *Oecologia*, *110*, 301–311, 1997.

Buchmann, N., J. R. Brooks, L. B. Flanagan, and J. Ehleringer, Carbon isotope discrimination of terrestrial ecosystems discrimination of terrestrial ecosystems, in *Stable Isotopes*, edited by H. Griffiths, pp. 203–221, BIOS Sci., Oxford, UK, 1998.

Ciais, P., P. P. Tans, J. W. C. White, M. Trolier, R. J. Francey, J. A. Berry,

D. A. Randall, P. J. Seller, J. G. Collatz, and D. S. Schimel, Partitioning ocean and land uptake of CO_2 as inferred by $\delta^{13}C$ measurements from the NOAA Climate Monitoring and Diagnostics Laboratory global air sampling network, *J. Geophys. Res.*, *100*(D3), 5051–5070, 1995.

Collatz, G. J., J. A. Berry, and J. S. Clark, Effects of climate and atmospheric CO_2 partial pressure on the global distribution of C-4 grasses: Present, past, and future, *Oecologia*, *114*, 441–454, 1998.

Doney, S. C., K. Lindsay, and J. K. Moore, Global ocean carbon cycle modeling, in *International JGOFS Synthesis*, edited by M. Fasham, Cambridge Univ. Press, New York, 2001.

Ehleringer, J. R., N. Buchmann, and L. B. Flanagan, Carbon isotope ratios in belowground carbon cycle processes, *Ecol. Appl.*, *10*(2), 412–422, 2000.

Ekblad, A., and P. Hogberg, Natural abundance of C-13 in CO_2 respired from forest soils reveals speed of link between tree photosynthesis and root respiration, *Oecologia*, *127*, 305–308, 2001.

Enting, I. G., On the use of smoothing splines to filter CO_2 data, *J. Geophys. Res.*, *92*(D9), 10,977–10,984, 1987.

Esbensen, S. K., and Y. Kushnir, *The Heat Budget of the Global Ocean: An Atlas Based on Estimates From Surface Marine Observations*, Clim. Res. Inst., Oreg. State Univ., Corvallis, Oreg., 1981.

Evans, J. R., T. D. Sharkey, J. A. Berry, and G. D. Farquhar, Carbon isotope discrimination measured concurrently with gas exchange to investigate CO_2 diffusion in leaves of higher plants, *Aust. J. Plant Physiol.*, *13*, 281–292, 1986.

Farquhar, G. D., J. R. Ehleringer, and K. T. Hubick, Carbon isotope discrimination and photosynthesis, *Ann. Rev. Plant Physiol. Plant Mol. Biol.*, *40*, 503–537, 1989.

Field, C. B., J. T. Randerson, and C. M. Malmström, Ecosystem net primary production: Combining ecology and remote sensing, *Remote Sens. Environ.*, *51*(1), 74–88, 1995.

Flanagan, L. B., J. R. Brooks, G. T. Verney, S. C. Berry, and J. R. Ehleringer, Carbon isotope discrimination during photosynthesis and the isotopic ratio of respired CO_2 in boreal forest ecosystems, *Global Biogeochem. Cycles*, *10*(4), 629–640, 1996.

Flanagan, L. B., J. R. Brooks, and J. R. Ehleringer, Photosynthesis and carbon isotope discrimination in boreal forest ecosystems: A comparison of functional characteristics in plants from three mature forest types, *J. Geophys. Res.*, *102*(D24), 28,861–28,869, 1997.

Francey, R. J., P. P. Tans, C. E. Allison, I. G. Enting, J. W. C. White, and M. Trolier, Changes in oceanic and terrestrial carbon uptake since 1982, *Nature*, *373*, 326–330, 1995.

Francey, R. J., C. E. Allison, D. M. Etheridge, C. M. Trudinger, I. G. Enting, M. Leuenberger, R. L. Langenfelds, E. Michel, and L. P. Steele, A 1000-year high precision record of $\delta^{13}C$ in atmospheric CO_2, *Tellus, Ser. B*, *51*, 170–193, 1999.

French, N. H. F., E. S. Kasischke, B. J. Stocks, J. P. Mudd, D. L. Martell, and B. S. Lee, Carbon release from fires in the North American boreal forest, in *Fire, Climate, and Carbon Cycling in the Boreal Forest*, edited by E. S. Kasischke and B. J. Stocks, pp. 377–388, Springer-Verlag, New York, 2000.

Frolking, S., Sensitivity of spruce/moss boreal forest net ecosystem productivity to seasonal anomalies in weather, *J. Geophys. Res.*, *102*(D24), 29,053–29,064, 1997.

Fung, I. Y., J. John, J. Lerner, E. Matthews, M. Prather, L. P. Steele, and P. J. Fraser, Three-dimensional model synthesis of the global methane cycle, *J. Geophys. Res.*, *96*(D7), 13,033–13,065, 1991.

Fung, I. Y., et al., Carbon 13 exchange between the atmosphere and biosphere, *Global Biogeochem. Cycles*, *11*(4), 507–533, 1997.

Gower, S. T., C. J. Kucharik, and J. M. Norman, Direct and indirect estimation of leaf area index, f(APAR), and net primary production of terrestrial ecosystems, *Remote Sens. Environ.*, *70*(1), 29–51, 1999.

Gruber, N., and C. D. Keeling, An improved estimate of the isotopic air-sea disequilibrium of CO_2: Implications for the oceanic uptake of anthropogenic CO_2, *Geophys. Res. Lett.*, *28*(3), 555–558, 2001.

Gruber, N., C. D. Keeling, R. B. Bacastow, P. R. Guenther, T. J. Lueker, M. Wahlen, H. A. J. Meijer, W. G. Mook, and T. F. Stocker, Spatiotemporal patterns of carbon-13 in the global surface oceans and the oceanic Suess effect, *Global Biogeochem. Cycles*, *13*(2), 307–335, 1999.

Hayes, J. M., Factors controlling ^{13}C contents of sedimentary organic compounds: Principles and evidence, *Mar. Geol.*, *113*(1–2), 111–125, 1993.

Heimann, M., C. D. Keeling, and C. J. Tucker, A three-dimensional model of atmospheric CO_2 transport based on observed winds, 3, Seasonal cycle and synoptic timescale variations, in *Aspects of Climate Variability in the Pacific and the Western Americas*, *Geophys. Monogr. Ser.*, vol. 55, edited by D. H. Peterson, pp. 277–303, AGU, Washington, D. C., 1989.

Heimann, M., et al., Evaluations of terrestrial carbon cycle models through simulations of the seasonal cycle of atmospheric CO_2: First results of a model intercomparison study, *Global Biogeochem. Cycles*, *12*(1), 1–24, 1998.

Kaminski, T., R. Giering, and M. Heimann, Sensitivity of the seasonal cycle of CO_2 at remote monitoring stations with respect to seasonal surface exchange fluxes determined with the adjoint of an atmospheric transport model, *Phys. Chem. Earth*, *21*, 457–462, 1996.

Kaminski, T., W. Knorr, M. Heimann, and P. Rayner, Assimilating atmospheric data into a terrestrial biosphere model: A case study of the seasonal cycle, *Global Biogeochem. Cycles*, *16*, 10.1029/2001GB001463, in press, 2002.

Keeling, C. D., The concentration and isotopic abundances of carbon dioxide in rural areas, *Geochim. Cosmochim. Acta*, *13*, 322–334, 1958.

Keeling, C. D., The concentration and isotopic abundances of carbon dioxide in rural and marine air, *Geochim. Cosmochim. Acta*, *24*, 277–298, 1961.

Keeling, C. D., W. G. Mook, and P. P. Tans, Recent trends in the $^{13}C/^{12}C$ ratio of atmospheric carbon dioxide, *Nature*, *277*, 121–123, 1979.

Keeling, C. D., T. P. Whorf, M. Wahlen, and J. van der Plicht, Interannual extremes in the rate of rise of atmospheric carbon dioxide since 1980, *Nature*, *375*, 666–669, 1995.

Kloeppel, B. D., S. T. Gower, I. W. Treichel, and S. Kharuk, Foliar carbon isotope discrimination in Larix species and sympatric evergreen conifers: A global comparison, *Oecologia*, *114*, 153–159, 1998.

Knorr, W., and M. Heimann, Impact of drought stress and other factors on seasonal land biosphere CO_2 exchange studied through an atmospheric tracer transport model, *Tellus, Ser. B*, *47*, 471–489, 1995.

Korner, C., G. D. Farquhar, and S. C. Wong, Carbon isotope discrimination by plants follows latitudinal and altitudinal trends, *Oecologia*, *88*, 30–40, 1991.

Leemans, R., and W. P. Cramer, The IIASA database for mean monthly values of temperature, precipitation and cloudiness of a global terrestrial grid, *WP-41*, 60 pp., Int. Inst. of Appl. Sys. Anal., Laxenburg, Austria, 1990.

Lloyd, J., and G. D. Farquhar, ^{13}C discrimination during CO_2 assimilation by the terrestrial biosphere, *Oecologia*, *99*, 201–215, 1994.

Lloyd, J., and J. A. Taylor, On the temperature dependence of soil respiration, *Func. Ecol.*, *8*, 315–323, 1994.

Lloyd, J., et al., Vegetation effects on the isotopic composition of atmospheric CO_2 at local and regional scales: Theoretical aspects and a comparison between rain forest in Amazonia and a boreal forest in Siberia, *Aust. J. Plant Physiol.*, *23*, 371–399, 1996.

Lloyd, J., et al., Vertical profiles, boundary layer budgets, and regional flux estimates for CO_2 and its $^{13}C/^{12}C$ ratio and for water vapor above a forest/bog mosaic in central Siberia, *Global Biogeochem. Cycles*, *15*(2), 267–284, 2001.

Marland, G., T. Boden, and R. J. Andres, Global, regional, and national annual CO_2 emissions from fossil-fuel burning, hydraulic cement production, and gas flaring: 1751-1998, *NDP 030*, Carbon Dioxide Inf. and Anal. Cent., Oak Ridge, Tenn., 2000.

Montieth, J. L., Solar radiation and productivity in tropical ecosystems, *J. Appl. Ecol.*, *9*, 747–766, 1972.

Mook, W. G., M. Koopmans, A. F. Carter, and C. D. Keeling, Seasonal, latitudinal, and secular variations in the abundance and isotopic-ratios of atmospheric carbon-dioxide, 1, Results from land stations, *J. Geophys. Res.*, *88*(C15), 915–933, 1983.

Nakazawa, T., S. Sugawara, G. Inoue, T. Machida, S. Makshyutov, and H. Mukai, Aircraft measurements of the concentrations of CO_2, CH_4, N_2O, and CO and the carbon and oxygen isotopic ratios of CO_2 in the troposphere over Russia, *J. Geophys. Res.*, *102*(D3), 3843–3859, 1997.

Press, W. H., B. P. Flannery, S. A. Teukolsky, and W. T. Vetterling, *Numerical Recipes in C: The Art of Scientific Computing*, Cambridge Univ. Press, New York, 1992.

Quay, P. D., B. Tilbrook, and C. S. Wong, Oceanic uptake of fossil-fuel CO_2–^{13}C evidence, *Science*, *256*(5053), 74–79, 1992.

Raich, J. W., and C. S. Potter, Global patterns of carbon dioxide emissions from soils, *Global Biogeochem. Cycles*, *9*(1), 23–36, 1995.

Raich, J. W., and W. H. Schlesinger, The global carbon dioxide flux in soil respiration and its relationship to climate, *Tellus, Ser. B*, *44*, 81–99, 1992.

Randerson, J. T., M. V. Thompson, T. J. Conway, I. Y. Fung, and C. B. Field, The contribution of terrestrial sources and sinks to trends in the seasonal cycle of atmospheric carbon dioxide, *Global Biogeochem. Cycles*, *11*(4), 535–560, 1997.

Rayner, P. J., I. G. Enting, R. J. Francey, and R. Langenfelds, Reconstructing the recent carbon cycle from atmospheric CO_2, $\delta^{13}C$ and O_2/N_2 observations, *Tellus, Ser. B*, *51*, 213–232, 1999.

Rotty, R. M., Estimates of seasonal variation in fossil fuel CO_2 emissions, *Tellus, Ser. B*, *39*, 184–202, 1987.

Ruimy, A., B. Saugier, and G. Dedieu, Methodology for the estimation of terrestrial net primary production from remotely sensed data, *J. Geophys. Res.*, *99*(D3), 5263–5283, 1994.

Running, S. W., and E. R. Hunt, Generalization of a forest ecosystem process model for other biomes, BIOME-BGC, and an application for global-scale models, in *Scaling Physiological Processes: Leaf to Globe*, edited by J. R. Ehleringer and C. B. Field, pp. 141–158, Academic, San Diego, Calif., 1993.

Runyon, J., and R. H. Waring, Environmental limits on net primary production and light use efficiency across the Oregon transect, *Ecol. Appl.*, *4*(2), 226–237, 1994.

Ryan, M. G., Effects of climate change on plant respiration, *Ecol. Appl.*, *1*(2), 157–167, 1991.

Schmidt, M., R. Graul, H. Sartorius, and I. Levin, Carbon dioxide and methane in continental Europe: A climatology, and ^{222}Radon-based emission estimates, *Tellus, Ser. B*, *48*, 457–473, 1996.

Schwarz, A. G., and R. E. Redmann, C4 grasses from the boreal forest region of northwestern Canada, *Can. J. Bot.*, *66*, 2424–2430, 1988.

Sellers, P. J., C. J. Tucker, G. J. Collatz, S. O. Los, C. O. Justice, D. A. Dazlich, and D. A. Randall, A global $1^\circ \times 1^\circ$ NDVI data set for climate studies, 2, The generation of global fields of terrestrial biophysical parameters from the NDVI, *Int. J. Remote Sens.*, *15*(17), 3519–3545, 1994.

Sokal, R. R., and F. J. Rohlf, *Biometry*, 859 pp., W. H. FreemanNew York, 1980.

Still, C., J. Berry, and J. Collatz, Global distribution of C_3 and C_4 vegetation: Carbon cycle implications, *Global Biogeochem. Cycles*, *16*, 10.1029/2001GB001807, in press, 2002.

Szumigalski, A. R., and S. E. Bayley, Net above-ground primary production along a bog-rich fen gradient in central Alberta, Canada, *Wetlands*, *16*(4), 467–476, 1996.

Takahashi, T., R. A. Feely, R. F. Weiss, R. H. Wanninkhof, D. W. Chipman, S. C. Sutherland, and T. T. Takahashi, Global air-sea flux of CO2: An estimate based on measurements of sea-air pCO_2 difference, *Proc. Natl. Acad. Sci. U. S. A.*, *94*(16), 8292–8299, 1997.

Tans, P. P., J. A. Berry, and R. F. Keeling, Oceanic $^{13}C/^{12}C$ observations: A new window on ocean CO_2 uptake, *Global Biogeochem. Cycles*, *7*(2), 353–368, 1993.

Tieszen, L. L., B. C. Reed, N. B. Bliss, B. K. Wylie, and D. D. DeJong, NDVI, C-3 and C-4 production, and distributions in great plains grassland land cover classes, *Ecol. Appl.*, *7*(1), 59–78, 1997.

Trolier, M., J. W. C. White, P. P. Tans, K. A. Masarie, and P. A. Gemery, Monitoring the isotope composition of atmospheric CO_2: Measurements from the NOAA Global Air Sampling Network, *J. Geophys. Res.*, *101*(D20), 25,897–25,916, 1996.

Wanninkhof, R., Relationship between wind speed and gas exchange over the ocean, *J. Geophys. Res.*, *97*(C5), 7373–7382, 1992.

Yakir, D., and X.-F. Wang, Fluxes of CO_2 and water between terrestrial vegetation and the atmosphere estimated from isotopic measurements, *Nature*, *380*, 515–517, 1996.

Zahn, A., R. Neubert, and U. Platt, Fate of long-lived trace species near the Northern Hemispheric tropopause, 2, Isotopic composition of carbon dioxide ((CO_2)-C-13, (CO_2)-C-14, and (COO)-O-18-O-16), *J. Geophys. Res.*, *105*(D5), 6719–6735, 2000.

Zaucker, F., P. H. Daum, U. Wetterauer, C. Berkowitz, B. Kromer, and W. S. Broecker, Atmospheric Rn-222 measurements during the 1993 NARE intensive, *J. Geophys. Res.*, *101*(D22), 29,149–29,164, 1996.

Zhang, J., P. D. Quay, and D. O. Wilbur, Carbon-isotope fractionation during gas-water exchange and dissolution of CO_2, *Geochim. Cosmochim. Acta*, *59*, 107–114, 1995.

J. J. Balle, I. Y. Fung, and C. J. Still, Center for Atmospheric Sciences, University of California, Berkeley, McCone Hall, Rm. 4767, Berkeley, CA 94720-4767, USA. (Johannaballe@aol.com; inez@sequoia.atmos.berkeley.edu; still@sequoia.atmos.berkeley.edu)

T. J. Conway and P. P. Tans, Climate Monitoring and Diagnostics Laboratory, NOAA, 325 Broadway, R/CMDL1, Boulder, CO 80305, USA. (Thomas.J.Conway@noaa.gov; Pieter.Tans@noaa.gov)

A. S. Denning and N. Suits, Department of Atmospheric Sciences, Colorado State University, Fort Collins, CO 80523, USA. (denning@atmos.colostate.edu; nsuits@atmos.colostate.edu)

S. C. Doney, Climate and Global Dynamics, National Center for Atmospheric Research, P.O. Box 3000, 1850 Table Mesa Drive, Boulder, CO 80307, USA. (doney@mar.ucar.edu)

J. T. Randerson, Divisions of Geological and Planetary Sciences and Engineering and Applied Science, California Institute of Technology, Mail Stop 100-23, Pasadena, CA 91125, USA. (jimr@gps.caltech.edu)

B. Vaughn and J. W. C. White, Institute of Arctic and Alpine Research, University of Colorado, Campus Box 450, Boulder, CO 80309-0450, USA. (bruce.vaughn@colorado.edu; James.White@colorado.edu)